Int. J. Heat Mass Transfer. Vol. 36, No. 11, pp. 2847–2859, 1993
Printed in Great Britain

0017–9310/93 $6.00+0.00

An investigation of transient mixed convection heat transfer of cold water in a tall vertical annulus with a heated rotating inner cylinder

C. J. HO† and F. J. TU
Department of Mechanical Engineering, National Cheng Kung University, Tainan, Taiwan 701, R.O.C.

(*Received* 24 *August* 1992 *and in final form* 19 *October* 1992)

Abstract—The transient buoyant rotating convective flow and heat transfer in a tall vertical annulus containing cold water near the density inversion have been investigated via a finite difference procedure. Simulations are carried out by solving axisymmetric Navier–Stokes equations adhering to the Boussinesq approximation coupled to the energy equation for an aspect ratio $A = 8$ and radius ratio $RR = 2$, two density inversion parameters $\theta_m = 0.4$ and 0.5, three Reynolds numbers $Re = 50$, 100, and 150, and varying Rayleigh number (up to 10^6). Numerical results demonstrate that the transient mixed convective flow and heat transfer may evolve into sustained oscillation over a certain range of Rayleigh number at given θ_m and Re; outside such unstable Ra-range, the transient evolution converges to steady-state solution. The transition into oscillatory convection arises at higher Rayleigh number with higher Reynolds number. Within the unstable convection regimes, simple as well as complex periodic oscillation, and chaotic oscillations have been detected. Moreover, the unstable Ra-ranges under fixed Re for $\theta_m = 0.5$ are found to be wider than those for $\theta_m = 0.4$, clearly reflecting the effects of the density inversion on the transient buoyant rotating convective flow and heat transfer in the tall vertical annulus.

INTRODUCTION

BUOYANCY driven flow and heat transfer of cold water in a confined space are well known to develop in a peculiar way due to the density inversion phenomenon associated with the occurrence of the maximum density at about 4°C [1–3]. Despite the great attention paid in the literature to the steady-state convection heat transfer problem of cold water, the transient flow condition has not yet been sufficiently studied. In the present paper we consider the transient axisymmetric buoyant rotating fluid flow and heat transfer of cold water enclosed in a tall vertical annulus with a heated rotating inner cylinder, as depicted schematically in Fig. 1. As demonstrated in the earlier study [4] for the steady-state solutions to a physical configuration identical to that under consideration here, the steady-state fluid flow structure and heat transfer characteristics of cold water within the vertical annulus can be greatly modified by the centrifugally forced convection due to the perturbing rotation of the inner cylinder. The resulting mixed convection heat and fluid flow fields in the vertical annulus are strongly affected by the density anomaly of cold water as well. In particular, the perturbing rotation of the inner cylinder can be a feasible treatment to circumvent occurrence of inherently minimum natural-convection heat transfer characteristics of cold water in a vertical annulus. The primary objective of this study is, as a continuing effort of our earlier study [4], to document the transient evolution to steady-state solutions and the transition to unsteady solutions of the buoyant rotating convection in a cold water-filled vertical annulus of aspect ratio 8.

The problem of fluid flow instability between concentric rotating cylinders, Taylor–Couette flow, has been studied extensively for over one hundred years and still remains as one of the hot topics for researchers. Comprehensive reviews of this flow problem are available [5, 6] and the references therein

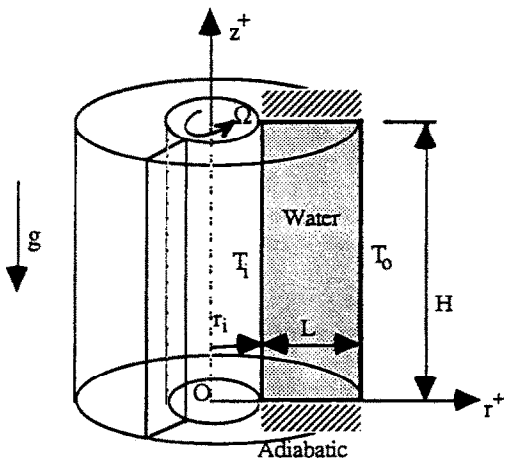

FIG. 1. Schematic diagram and coordinate system of the physical configuration.

† To whom correspondence should be addressed.

NOMENCLATURE

a	exponent of density equation
A	aspect ratio, H/L
Fo	Fourier number, $\alpha t/L^2$
Fr	Froude number, $L\Omega^2/g$
g	gravitational acceleration
Gr	Grashof number, $g(rsp)\lvert T_i-T_o\rvert^a L^3/(\nu^2)$
h	heat transfer coefficient
H	height of the annulus
k	thermal conductivity
k_{eq}	equivalent thermal conductivity, $Nu\ln(RR)/(RR-1)$
L	annulus gap, r_o-r_i
Nu	Nusselt number
Pr	Prandtl number
r^+	radial coordinate
r	dimensionless radial coordinate, r^+/L
Ra	Rayleigh number, $Pr\,Gr$
Re	rotational Reynolds number, $L\Omega^2/\nu$
r_i	radius of inner cylinder
r_o	radius of outer cylinder
RR	radius ratio, r_o/r_i
rsp	coefficient of density equation
T	temperature
u	radial velocity component, $-(1/r)(\partial\psi/\partial z)$
v	angular velocity component
w	axial velocity component, $(1/r)(\partial\psi/\partial r)$
z^+	axial coordinate
z	dimensionless axial coordinate, z^+/L.

Greek symbols

α	thermal diffusivity
Γ	swirl velocity, rv
ζ	dimensionless vorticity, $(\partial u/\partial z)-(\partial w/\partial r)$
θ	dimensionless temperature, $(T-T_o)/(T_i-T_o)$
θ_m	density inversion parameter, $(T_m-T_o)/(T_i-T_o)$
ν	kinematic viscosity
ρ	density
τ	dimensionless time, $Pr\,Re\,Fo$
ψ^+	stream function
ψ	dimensionless stream function, $\psi^+/(L^3\Omega)$
Ω	rotational speed of inner cylinder.

Subscripts

i	inner cylinder
m	density extreme
o	outer cylinder.

Superscript

$\overline{\ }$	averaged quantity.

should be consulted for further details. Owing to its relevance to various engineering applications and geophysical phenomena, there has been considerable research interest toward the buoyant rotating (mixed) convection flow and heat transfer within a rotating cylindrical annulus, as listed chronically in refs. [7–12]. de Vahl Davis and his coworkers [7, 8] analyzed, through finite difference calculations, laminar mixed convection heat transfer for short to moderate vertical annuli with an inner cylinder and one of the horizontal endwalls rotating about the vertical axis. Furthermore, Ball and Farouk presented a series of studies [9–12] concerning the buoyancy effects on the fluid flow patterns and heat transfer characteristics developed in a taller annulus with a heated rotating inner cylinder. In particular, the buoyancy effects on the bifurcation and stability of the Taylor–Couette flow were respectively addressed numerically [11] and experimentally [12]. The structure of the Taylor vortices was found to be greatly distorted with buoyant flows.

PROBLEM DESCRIPTION AND FORMULATION

We consider a vertical cylindrical annulus of height H and gap width L formed by two concentric vertical circular cylinders of radii r_i and r_o, respectively. As depicted in Fig. 1, the inner and outer cylinders are maintained isothermally at temperature T_i and T_o ($<T_i$), respectively. The heated inner cylinder rotates axially with a constant angular speed Ω, while the outer cylinder and the horizontal end walls of the annulus are stationary. Moreover, the horizontal end walls are assumed adiabatic.

The mathematical formulation for the problem considered here is essentially identical to that described in detail in the earlier work [4]; therefore, there is no need to repeat it here. In short, the transient axisymmetric, laminar buoyant rotating fluid flow and heat transfer of cold water in the annulus are governed by the following dimensionless differential equations for the vorticity ζ, the stream function ψ, the swirl velocity Γ, and the temperature θ:

$$\frac{1}{Pr\,Re}\frac{\partial\zeta}{\partial Fo}+\frac{\partial(u\zeta)}{\partial r}+\frac{\partial(w\zeta)}{\partial z}-\frac{Gr\,Fr}{Re^2}\left(\Gamma\frac{\partial\theta^*}{\partial z}+2\theta^*\frac{\partial\Gamma}{\partial z}\right)-\frac{2}{r^3}\frac{\partial\Gamma}{\partial z}+\frac{Gr}{Re^2}\frac{\partial\theta^*}{\partial r}=\frac{1}{Re}\left(\frac{\partial^2\zeta}{\partial r^2}+\frac{1}{r}\frac{\partial\zeta}{\partial r}-\frac{\zeta}{r}+\frac{\partial^2\zeta}{\partial z^2}\right) \quad (1)$$

$$\frac{\partial}{\partial r}\left(\frac{1}{r}\frac{\partial \psi}{\partial r}\right)+\frac{1}{r}\frac{\partial^2 \psi}{\partial z^2}=-\zeta \tag{2}$$

$$\frac{1}{Pr\,Re}\frac{\partial \Gamma}{\partial Fo}+\frac{1}{r}\frac{\partial (ru\Gamma)}{\partial r}+\frac{\partial (w\Gamma)}{\partial z}$$

$$=\frac{Gr\,Fr}{Re^2}\frac{u\theta^*\Gamma}{r}+\frac{1}{Re}\left(\frac{\partial^2\Gamma}{\partial r^2}-\frac{1}{r}\frac{\partial \Gamma}{\partial r}+\frac{\partial^2\Gamma}{\partial z^2}\right) \tag{3}$$

$$\frac{1}{Pr\,Re}\frac{\partial \theta}{\partial Fo}+\frac{1}{r}\frac{\partial (ru\theta)}{\partial r}+\frac{\partial (w\theta)}{\partial z}$$

$$=\frac{1}{Pr\,Re}\left(\frac{\partial^2\theta}{\partial r^2}-\frac{1}{r}\frac{\partial \theta}{\partial r}+\frac{\partial^2\theta}{\partial z^2}\right) \tag{4}$$

where $\theta^*=|\theta-\theta_m|^a$ and the density–temperature relationship of cold water proposed by Gebhart and Mollendrof [13] was adopted as of the form:

$$\rho(T)=\rho_m(1-rsp|T-T_m|^a) \tag{5}$$

where $\rho_m=999.9720$ kg m^{-3}, $T_m=4.29325$°C, $a=1.894816$, and $rsp=9.297173\times10^{-6}$ (°C)$^{-a}$.

The dimensionless boundary conditions are:

$$z=0 \text{ or } A;\quad u=w=\Gamma=\psi=0,\quad \frac{\partial\theta}{\partial z}=0 \tag{6a}$$

$$r=\frac{1}{RR-1};$$

$$u=w=\psi=0,\quad \Gamma=\frac{1}{(RR-1)^2},\quad \theta=1 \tag{6b}$$

$$r=\frac{RR}{RR-1};$$

$$u=w=\Gamma=\psi=\theta=0. \tag{6c}$$

The local Nusselt numbers on the inner and outer cylinders of the annulus are, respectively, defined as

$$Nu_i=\frac{h_iL}{k}=-\left.\frac{\partial\theta}{\partial r}\right|_{r=1/(RR-1)} \tag{7a}$$

and

$$Nu_o=\frac{h_oL}{k}=\left.\frac{\partial\theta}{\partial r}\right|_{r=RR/(RR-1)}. \tag{7b}$$

NUMERICAL METHOD

Equations (1)–(4) subjected to the dimensionless boundary conditions, equation (6), were solved using a finite difference technique. The time derivatives were discretized using the forward differencing scheme while the spatial derivatives were discretized by the second-order central difference formula except the convective terms for which the two-dimensional QUICK scheme [14] was adopted. A line successive relaxation scheme was used to solve the finite difference equations for the vorticity, the swirl velocity, and the temperature of the problem; and the SOR scheme was employed for solving the equations for the stream function. A fully implicit scheme was used to attain the transient solutions with a relative convergence criterion of 10^{-4} for the iteration calculations at each time step.

In the present study, the spatial discretization in the radial direction was done in a non-uniform manner having denser grid distribution adjacent to both the vertical walls of the annulus; while uniform grid lines were laid in the axial direction. A spatial mesh of 31(radial) × 121(axial) was selected for the present calculations, which was found to be adequate through a series of tests for grid-size independence of the solutions. For instance, the temporal histories of the average Nusselt number at the inner cylinder for $\theta_m=0.4$, $Re=100$, $Ra=10^5$, and $A=8$ using three meshes of 31×121, 41×121, 31×161 were compared as shown in Fig. 2, and revealed little difference in the trend of the temporal variation for the Nusselt number. The quantitative difference between the average Nusselt number predicted by the 31×121 and 31×161 meshes

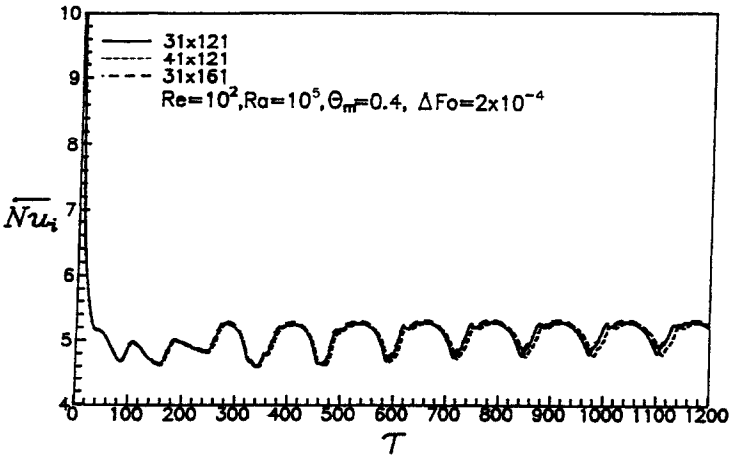

FIG. 2. Comparison of the averaged Nusselt number at the inner cylinder of the annulus for different meshes.

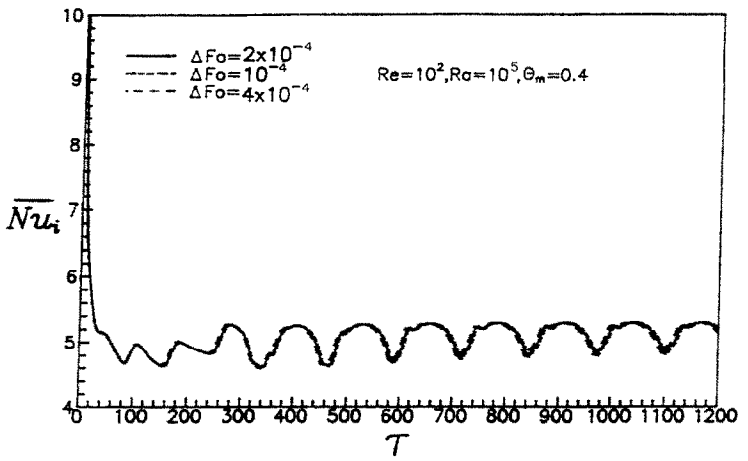

FIG. 3. Comparison of the average Nusselt number at the inner cylinder for using different time-step.

is 1.3% and between 31×121 and 41×121 meshes it is 0.4%. Furthermore, the differences in the frequency of the oscillation of the Nusselt number are 0.38% between the 31×121 and 31×161 meshes and 0.9% between the 31×121 and 41×121 meshes.

Moreover, time steps of 4×10^{-4}, 2×10^{-4}, and 10^{-4} were respectively, used for the transient calculations of $Re = 50$, 100, and 150, which were determined by means of a time step dependence study as exemplified in Fig. 3 comparing the results of the Nusselt number using time steps of 10^{-4}, 2×10^{-4}, and 4×10^{-4} for $A = 8$, $\theta_m = 0.4$, $Re = 100$, $Ra = 10^5$. Evidently, the three time steps yield quite identical temporal variations and the difference in the frequency of the oscillation is only 0.1% between time steps of 10^{-4} and 2×10^{-4}.

RESULTS AND DISCUSSION

Prior to performing parametric simulations, the transient computer code developed in the present study was validated by comparing the steady-state results converged from the present transient simulation model with the published data for two cases: the pure natural convection of cold water [2] and the buoyant rotating convection of air [9] in a vertical annulus. As demonstrated in Tables 1 and 2, the predicted steady-state Nusselt number and the equivalent thermal conductivity are in good agreement with the data in the references.

In the present work, all the transient simulations were initiated from cold start, namely the stagnant fluid at a uniform temperature of the cold wall, and the inner cylinder of the annulus was suddenly heated isothermally to a constant temperature with a constant rotating speed about the axis. Simulations have been carried out for cold water ($Pr = 12.5$) contained in a tall annulus of aspect ratio $A = 8$ and radius ratio $RR = 2$ to explore the evolution of fluid flow field and heat transfer characteristics over the following ranges of the governing physical parameters: $Re = 50$, 100, 150; $Ra = 5 \times 10^3$ to 10^6; $\theta_m = 0.4$ and 0.5 with $Fr = 0$. The selected values of the density inversion parameter θ_m for the present study were aimed to reflect the strong effect of the density inversion phenomenon on the fluid flow problem considered. Furthermore, the parameter Froude number Fr set to zero here follows the findings from the earlier studies [4, 7, 9] that the centrifugal and Coriolis components of the buoyancy force are rather negligible in comparison with that induced by the gravitational acceleration under the low rotational speed under consideration. The numerical results generated are presented hereafter to explore the prominent effects

Table 1. The Nusselt number and the maximum stream function for steady-state natural convection of cold water in a vertical annulus, $A = 1$, $RR = 2$, $\theta_m = 0.5$

Ra	$\overline{Nu}$	ψ_{max}
10^4	1.761(1.738)†	0.282(0.281)†
10^5	3.572(3.521)†	1.007(0.998)†
10^6	7.162(7.136)†	2.104(2.043)†

† From ref. [2].

Table 2. Average heat transfer results of the buoyant rotating convection of air in a vertical annulus of $A = 10$ with $Re = 100$ and $RR = 2$

Gr	$\overline{Nu}$	$\bar{k}_{eq}$
0	2.010	1.393(1.473)†
100	1.998	1.384(1.370)†
500	1.909	1.323(1.324)†
1000	1.811	1.255(1.258)†

† From ref. [9].

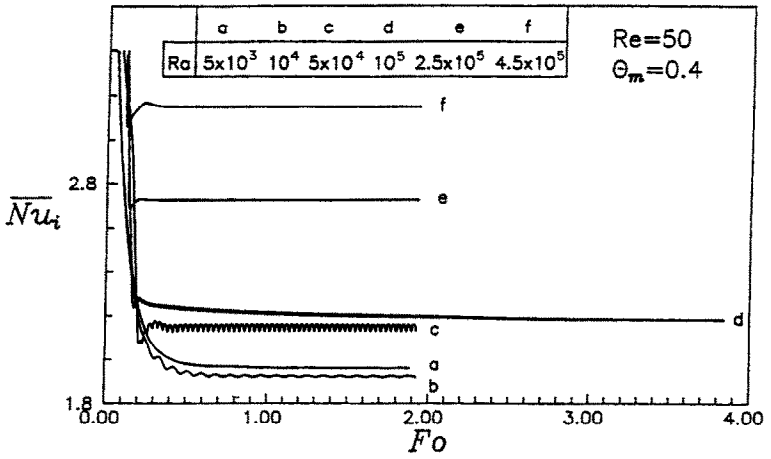

FIG. 4. Time-history of the average Nusselt number at the inner cylinder: $Re = 50$, $\theta_m = 0.4$.

of the Rayleigh number on the transient fluid flow and heat transfer across the annulus under the influence of the density inversion at three different Reynolds numbers considered.

Results for Re = 50

For $Re = 50$ and $\theta_m = 0.4$ with $Ra = 5 \times 10^3$ the flow and temperature fields of cold water in the annulus were found to converge gradually to the steady state, as evident in the time-history plot of the average Nusselt number on the inner cylinder presented in Fig. 4. The corresponding transient evolution of the flow field and temperature distribution inside the annulus is illustrated, respectively, by a sequence of contour maps of streamlines (left) and isotherms (right) in Fig. 5. It should be noted that in the contour plots shown, the rotating heated inner cylinder is on the left of the vertical annulus. The two numbers in the parentheses along with the streamline plots denote the extremes of the stream function. Moreover, the

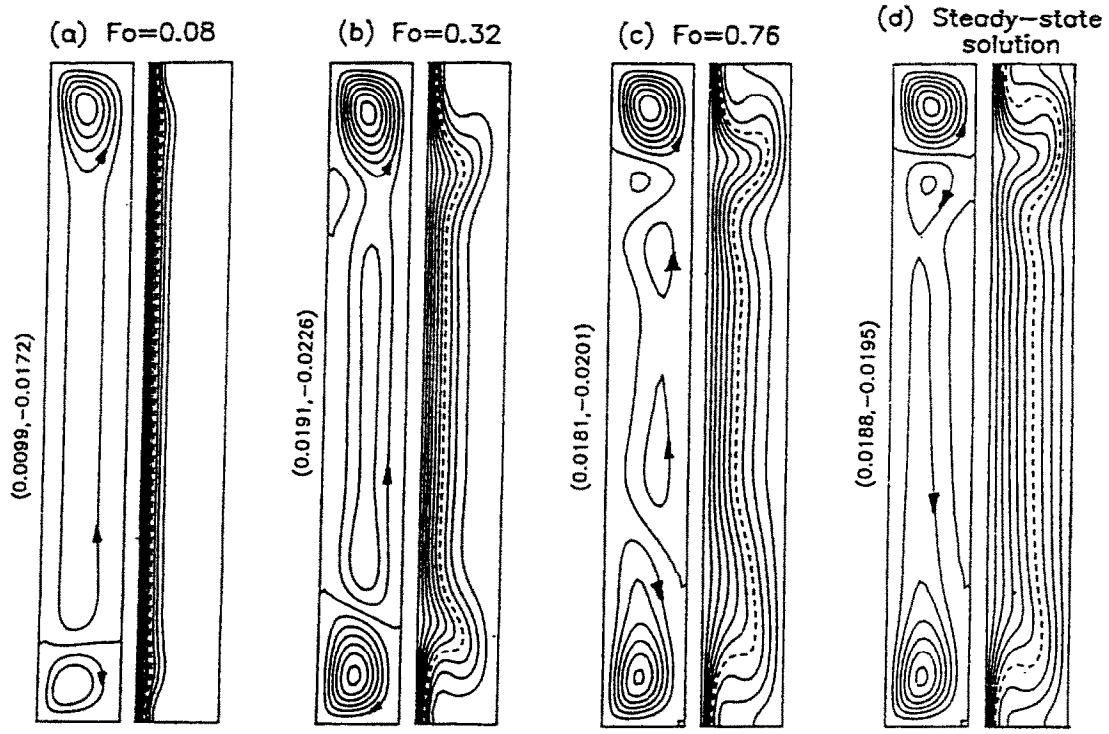

FIG. 5. Typical transient evolution of the streamlines (left) and isotherms (right) converged to steady-state solution for $\theta_m = 0.4$, $Re = 50$, and $Ra = 5000$.

temperature contour corresponding to the density extreme, θ_m is traced by a dashed line on the isotherm plots. The plots in Fig. 5 clearly illustrate the competing interaction of transient buoyancy-driven flow with the growing vortices induced by the centrifugal force near both the upper and bottom corners of the annulus; and a steady-state solution is attained at $Fo = 1.88$, featuring a complex multicellular flow structure dominated by the counter-rotating recirculations, respectively, at the top and bottom regions of the annulus, greatly distorting the isotherms. Similar to the finding obtained in ref. [4], the effects of the centrifugal force appear to be confined to the region between the heated inner cylinder and the isotherm contour of the density extreme θ_m. An increase of Ra up to 10^4 triggers a sustained simple periodic flow and temperature fields with a dimensionless frequency of 9.7, as demonstrated by the oscillatory variation of the average Nusselt number on the rotating inner cylinder shown in Fig. 4. Further, from Fig. 4 one can observe that the simple periodic oscillatory heat transfer behavior continues to sustain with

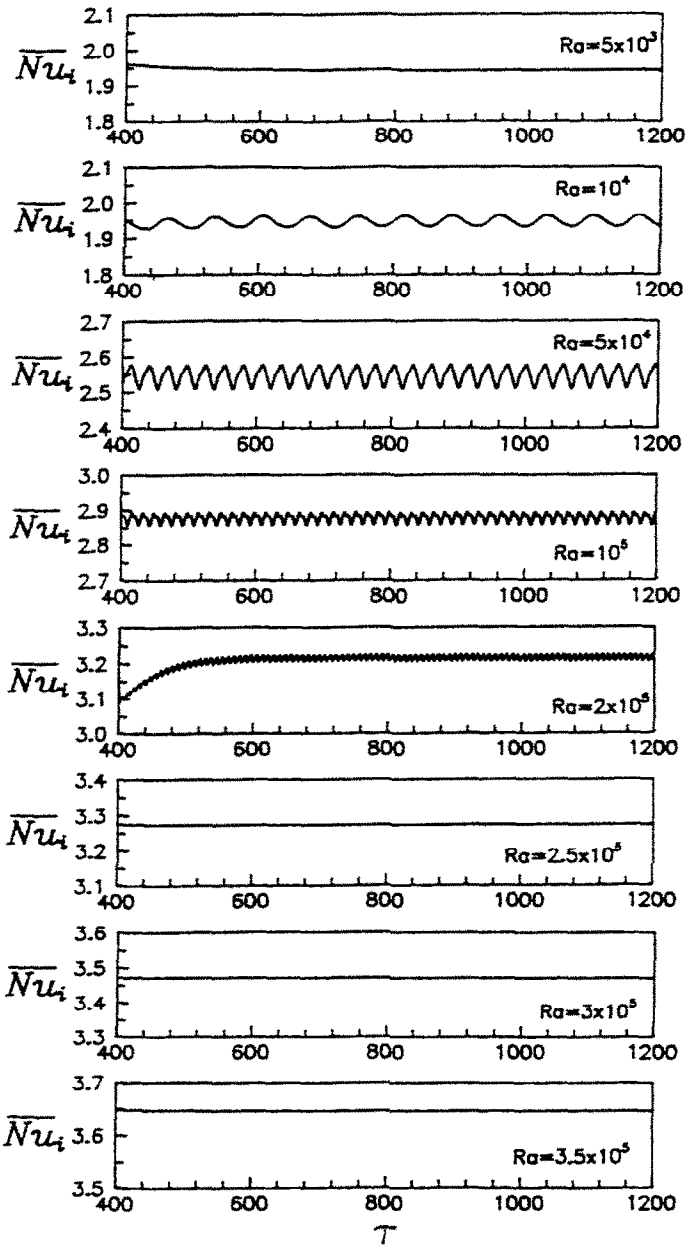

FIG. 6. The variations in the oscillation pattern of the averaged Nusselt number with the Rayleigh number for $\theta_m = 0.5$ and $Re = 50$.

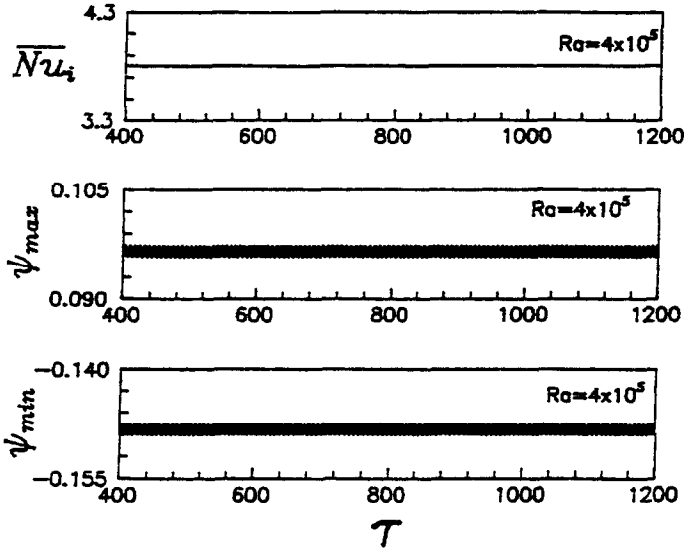

FIG. 7. The oscillation in the flow field after the averaged Nusselt number has attained a steady-state value: $Re = 50$, $\theta_m = 0.5$, and $Ra = 4 \times 10^5$.

increasing oscillation frequency but at decreasing amplitude as the Rayleigh number is increased to 10^5. Interestingly, at further higher Ra ($>2 \times 10^5$), as can be seen in Fig. 4, the oscillatory heat transfer behavior ceases to exist and a steady-state Nusselt number variation resumes after a transient period. In contrast to this reverse transition from unstable to steady-state heat transfer characteristics for $Ra > 2 \times 10^5$, it should be noted that the flow field of cold water inside the annulus still exhibits a sustained low-amplitude oscillation.

Similar to the foregoing for $\theta_m = 0.4$, the periodic oscillatory heat transfer behavior prevails for $\theta_m = 0.5$ in a certain range of Ra with Re fixed at 50. Figure 6 shows the transient Nusselt number variation over a range of Ra from 5×10^3 to 3.5×10^5. At $Ra = 5 \times 10^3$ a steady-state heat transfer behavior evolves. For $Ra = 10^4$ a periodic oscillation at a dimensionless frequency of 8.8 is detected. The oscillatory heat transfer characteristics continue to prevail at further increasing frequency but with decreasing amplitude as the Rayleigh number is increased up to $Ra = 2.5 \times 10^5$; thereabouts, a reverse transition to steady state regime is observed. Resembling that observed for $\theta_m = 0.4$, the flow fields inside the annulus continue to exhibit periodic oscillations with very small amplitude as demonstrated by the temporal evolution of the Nusselt number and the extremes of the stream function in Fig. 7 for $Ra = 4 \times 10^5$. Another important observation from the results for $Re = 50$ is that for $\theta_m = 0.4$

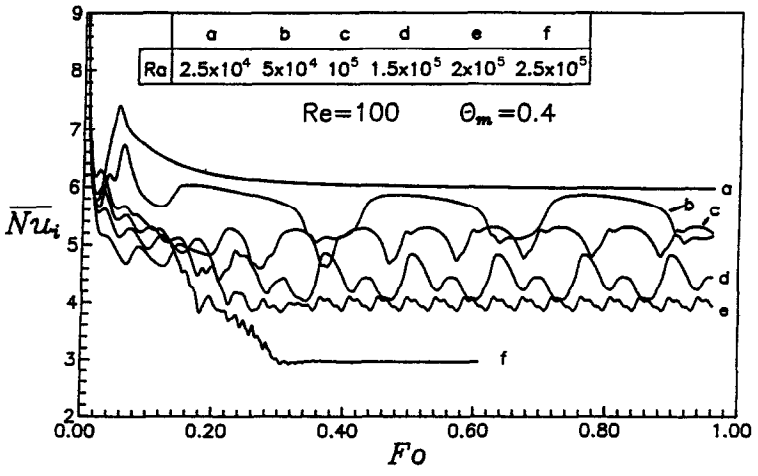

FIG. 8. Time-history of the average Nusselt number at the inner cylinder: $Re = 100$, $\theta_m = 0.4$.

and 0.5, the increase of Ra beyond a certain value leads to increasingly higher steady-state/periodically averaged Nusselt number, reflecting the aiding effects of the buoyancy force on the centrifugally forced convection heat transfer across the annulus.

Results for $Re = 100$

In general, the heat transfer characteristics and the flow fields in the annulus for $Re = 100$ are found to experience a transition quite similar to that elaborated above for $Re = 50$, when the Rayleigh number is varied over a certain Ra-range. The time-history of the heat transfer rate displayed in Fig. 8 for $\theta_m = 0.4$ clearly reveals a transition from the steady-state regime at $Ra = 2.5 \times 10^4$ into a periodic oscillation window for Ra between 5×10^4 and 2.45×10^5, and then a reverse transition to another steady state regime arises at $Ra = 2.5 \times 10^5$. Moreover, as demonstrated in Fig. 9 displaying the temporal evolution of the maximum and minimum stream function values of the mixed convective flow field, complex periodic oscillatory flow fields arise over the range of Ra between 5×10^4 and 2.45×10^5. To reveal more details about the flow structure and temperature distribution inside the annulus, Fig. 10(b) exemplifies the streamlines and isotherms at different time instants indicated in Fig. 10(a) over a cycle of the oscillatory Nusselt number for $Re = 100$ and $Ra = 2 \times 10^5$. Each frame of the streamlines plots in Fig. 10(b) features a staggered multicellular flow pattern filling the annulus. These layered counter-rotating vortices generally are seen to be demarcated in a manner following the wavy isotherm contour for the density extreme θ_m: the clockwise and counterclockwise vortices are centered to the left and right of the density extreme curve, respectively. This further signifies the vital role played by the density inversion on the development of the buoyant rotating convection in the annulus. During a cycle, the layered vortices are seen to shift upward from the bottom of the annulus, owing to generation

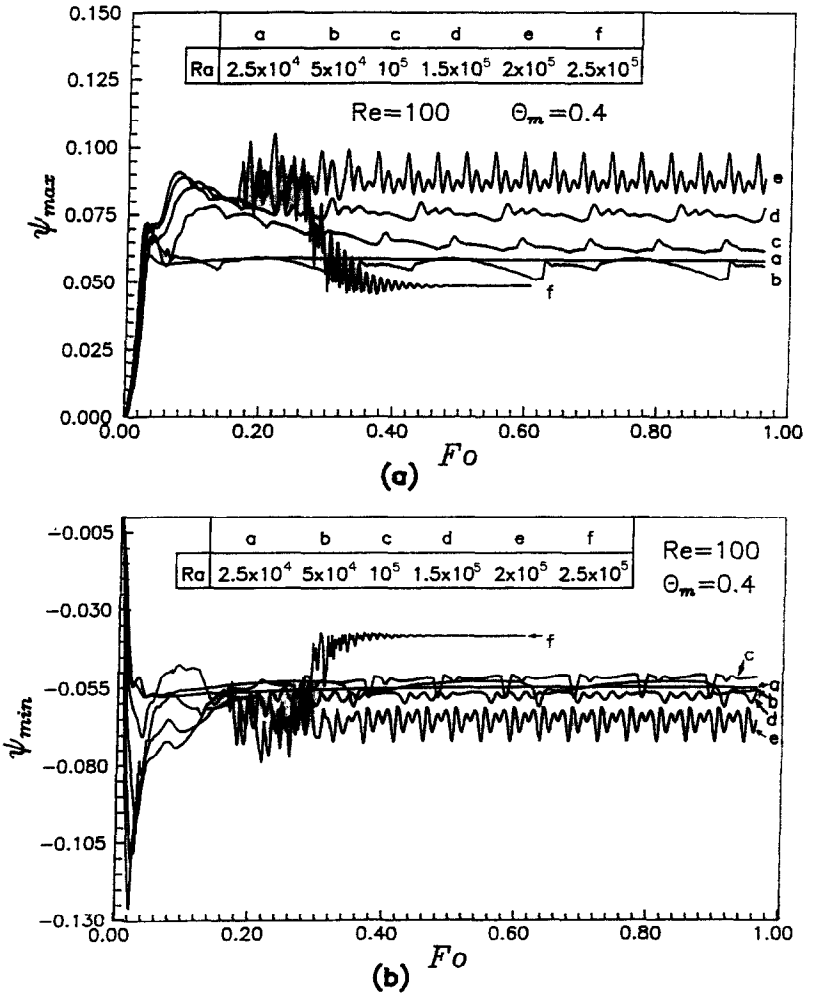

FIG. 9. Temporal variations for $Re = 100$ and $\theta_m = 0.4$ of (a) maximum and (b) minimum values of the stream function.

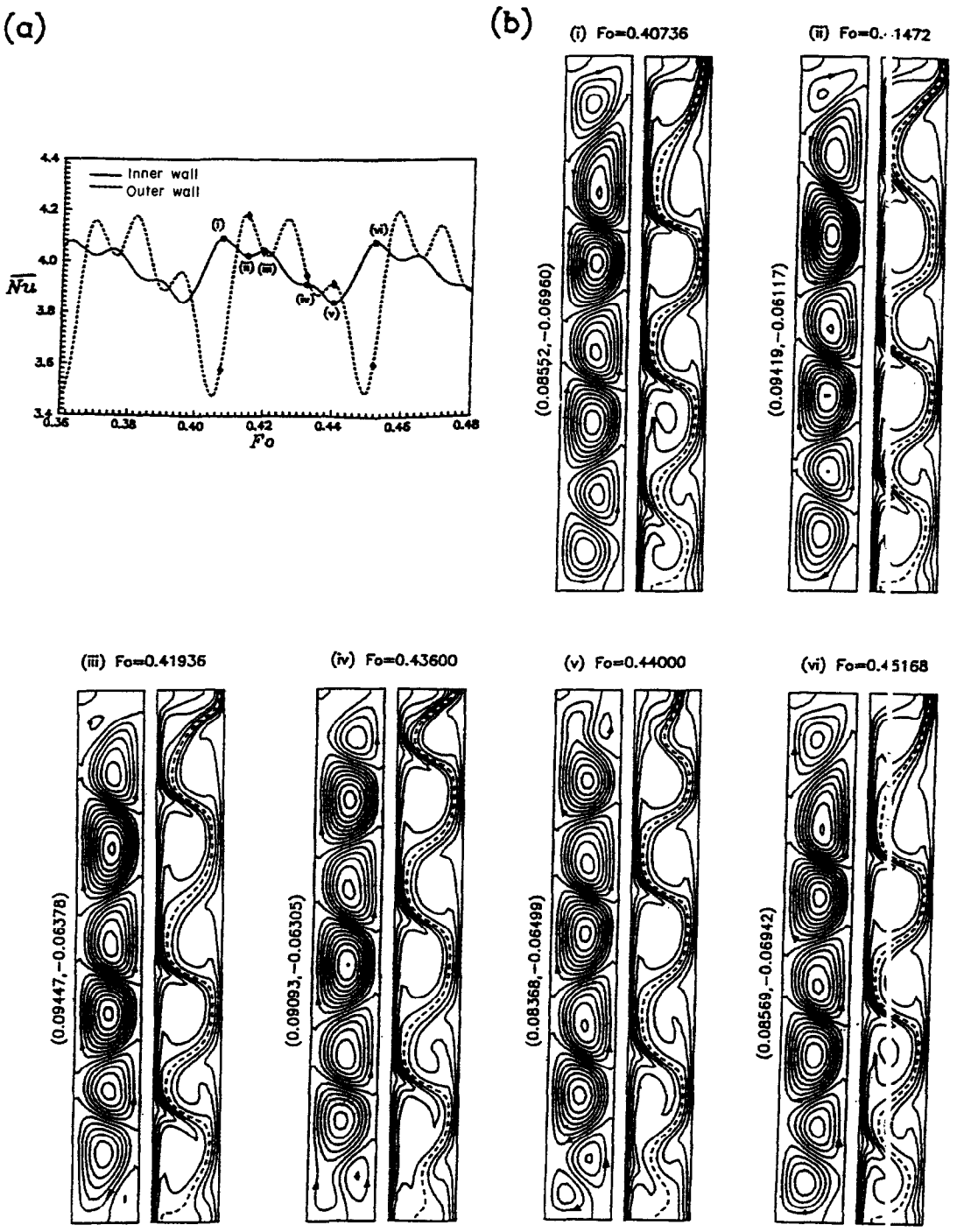

FIG. 10. Streamlines and isotherms at different time instants within a cycle of the oscillations for $Re = 100$, $\theta_m = 0.4$, and $Ra = 2 \times 10^5$.

or collapse of vortices in the end regions. Due to the intensified clockwise circulation near the bottom left corner, a new vortex is induced at the bottom right corner near the outer cylinder, meanwhile the clockwise vortex in the upper region is suppressed. The new growing counterclockwise vortex at the bottom region further results in split-up of the upward-shifting clockwise vortex near the inner cylinder. Further comparison of Fig. 8 with Fig. 4 indicates that contrary to that for $Re = 50$, the increase of Ra for $Re = 100$ and $\theta_m = 0.4$ results in a substantial drop of the steady-state/periodically averaged Nusselt number, indicative of the opposing effects of the increasing buoyancy force.

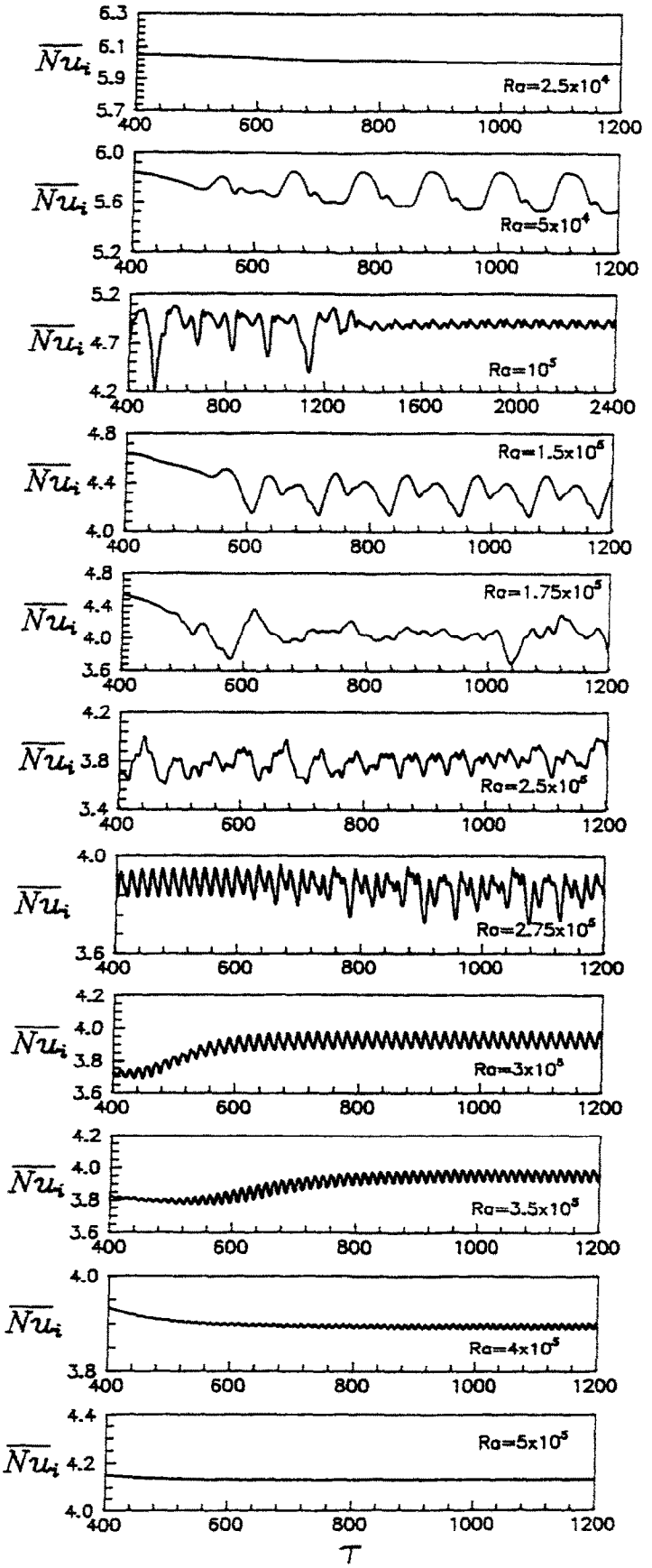

FIG. 11. Variations of the oscillation pattern of the averaged Nusselt number with the Rayleigh number for $\theta_m = 0.5$ and $Re = 100$.

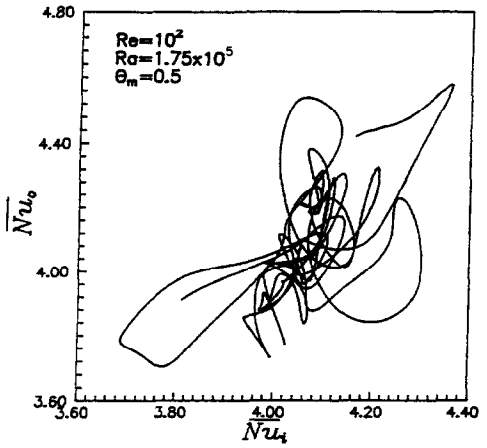

FIG. 12. Phase plot for a chaotic state at $Ra = 2 \times 10^5$ with $\theta_m = 0.5$ and $Re = 100$.

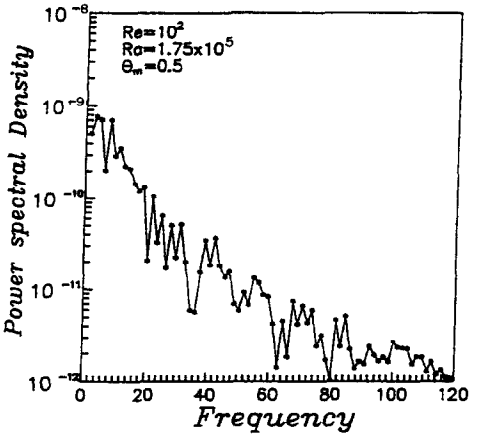

FIG. 13. Power spectrum of the averaged Nusselt number for $Ra = 2 \times 10^5$, $Re = 100$, and $\theta_m = 0.5$.

For $\theta_m = 0.5$, as shown in Fig. 11, the increase of Ra beyond 5×10^4 gives rise to a transition into the oscillatory heat transfer regime. In particular, at $Ra = 1.75 \times 10^5$ the oscillation becomes aperiodic or chaotic as demonstrated by the strange attractor behavior shown in the phase plot of $\overline{Nu_i}$ vs $\overline{Nu_o}$ in Fig. 12. Figure 13 further displays the corresponding power spectrum of the chaotic oscillation for the average Nusselt number on the inner cylinder. The aperiodic oscillation persists with further increase of Ra up to 2.75×10^5. But at $Ra = 3 \times 10^5$ a periodic oscillation heat transfer behavior reappears and continues to prevail with decaying amplitude when the Rayleigh number is further increased. Till $Ra = 5 \times 10^5$ another steady-state heat transfer resumes as indicated in Fig. 11.

Results for $Re = 150$

A transition displaying characteristics similar to those observed for $Re = 100$ are also found for $Re = 150$ over a certain range of Ra. As shown in the temporal variation of the average Nusselt number on the inner cylinder in Fig. 14 for $\theta_m = 0.4$, a periodic oscillation window between two steady-state heat transfer regimes is observed for Ra between 10^5 and 4×10^5 with the occurrence of a reverse transition from unstable to steady state at $Ra = 5 \times 10^5$. As for $\theta_m = 0.5$, the oscillatory heat transfer behavior can be detected for Ra in a wider range between 10^5 and 8×10^5 as illustrated in Fig. 15. There appears to be a noticeable difference for the transition evolution between the cases under $\theta_m = 0.5$ and those for $\theta_m = 0.4$. The transition through oscillatory heat transfer regime with increasing Ra for $\theta_m = 0.5$ first evolves as those found for $Re = 50$ and 100, increasingly higher oscillation frequency but at decaying amplitude with increasing Ra till about 4×10^5, at which a quasi-steady state heat transfer takes place. But at $Ra = 5 \times 10^5$, the heat transfer behavior evolves into a chaotic oscillation. Interestingly, with further

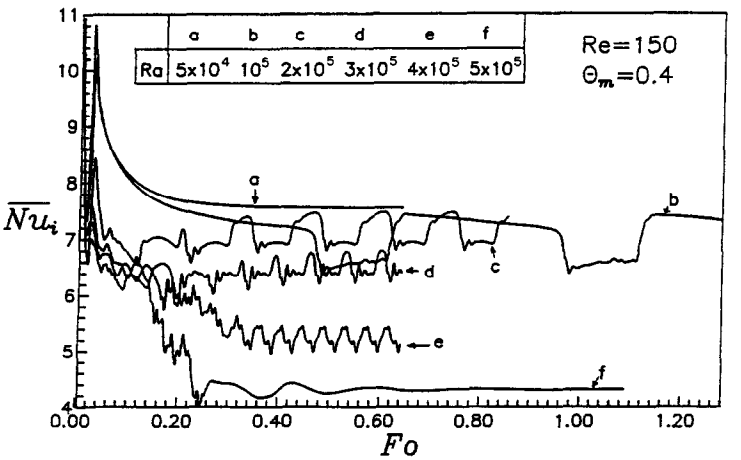

FIG. 14. Time-history of the averaged Nusselt number on the inner cylinder for $Re = 150$ and $\theta_m = 0.4$.

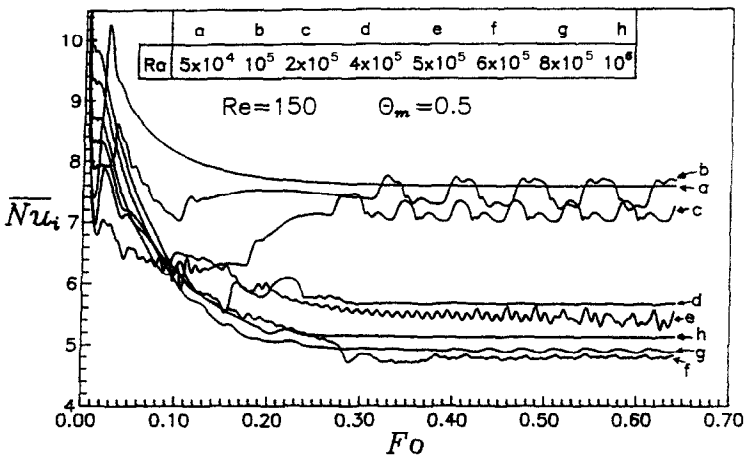

FIG. 15. Time series of the averaged Nusselt number on the inner cylinder for $Re = 150$ and $\theta_m = 0.5$.

increase of Ra, the aperiodicity is regularized turning into another periodic oscillation window as demonstrated in Fig. 16 displaying the power spectrums for $Ra = 5 \times 10^5$ and 6×10^5. Eventually, at $Ra = 10^6$ a reverse transition to the steady-state heat transfer behavior occurs.

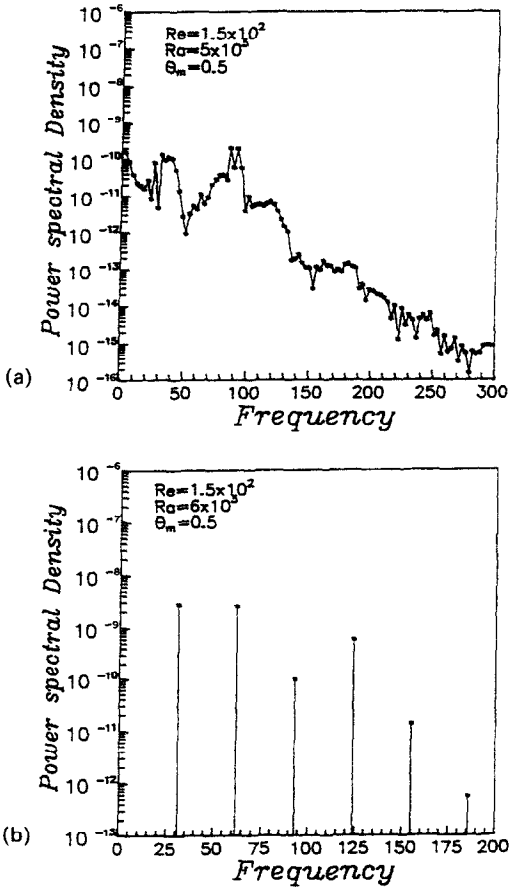

FIG. 16. Power spectrum of the averaged Nusselt number on the inner cylinder at $\theta_m = 0.5$, and $Re = 150$ with (a) $Ra = 5 \times 10^5$ and (b) $Ra = 6 \times 10^5$.

Finally, based on the transient computations performed in the present study, the effect of the Rayleigh and Reynolds numbers on the stability of the flow problem under consideration can be represented by a stability diagram of the form shown in Fig. 17. It is evident from the figure that for $\theta_m = 0.4$ and 0.5, the critical Rayleigh number for the transition into oscillatory heat transfer regime tends to increase with the increase of the Reynolds number, reflecting the stabilizing effect of the centrifugal force on the mixed

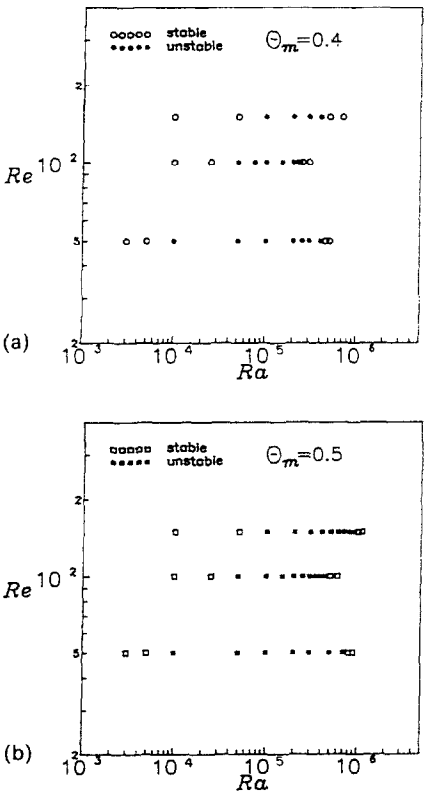

FIG. 17. Stability diagram of the buoyant rotating convection of cold water in the annulus.

convection in the annulus. Moreover, based on the slope of a straight line curve-fitted through the critical Rayleigh numbers entering the unstable windows in Fig. 17, a stability criterion can be postulated as of the form

$$\frac{Ra}{Re^{2.13}} \geqslant C(\approx 2.45). \quad (8)$$

The precise value of C in the relationship (8) still remains to be determined quantitatively through further detailed numerical simulations and/or by experiments. On the other end of the unstable Ra-range, the critical Rayleigh number for the reverse transition from unstable to stable regime does not exhibit such a simple relation with the Reynolds number. Further examination of Fig. 17 reveals that the Ra-ranges over which the oscillatory heat transfer prevails at fixed Re for $\theta_m = 0.5$ appear to be wider than those for $\theta_m = 0.4$, further indicative of the effect of density inversion on the transient buoyant rotating convection inside the tall annulus.

CONCLUDING REMARKS

The transient behavior of fluid flow and heat transfer produced by combined thermal buoyancy force (from radial thermal gradient) and centrifugal force (due to a rotating inner cylinder) in a tall annulus of aspect ratio 8 containing water near the density inversion has been studied via a numerical experiment. The simulations have been performed for two values of the density inversion parameter $\theta_m = 0.4$ and 0.5 at $Re = 50$, 100, and 150 with varying Rayleigh number. The present results demonstrate that the transient buoyant rotating convection of cold water across the tall annulus at fixed θ_m and Re may become unstable over a certain range of the Rayleigh number, within which simple as well as complex periodic (quasi-periodic) and chaotic (aperiodic) solutions have been found. The periodic oscillatory heat transfer behavior is generally characterized with an increasing frequency but at decaying amplitude with the increase of the Rayleigh number, so as to result in a reverse transition from unstable to steady-state regime with the Rayleigh number greater than another critical value. Furthermore, the Ra-ranges for $\theta_m = 0.5$ over which the instability arises are found to be wider than those for $\theta_m = 0.4$. Still, further detailed numerical work is needed to quantitatively predict the critical values for the transition; and as well, the experimental work verifying the numerical results is needed in future study.

Acknowledgement—The constructive comments of the reviewers are sincerely appreciated. The necessary computing facility and time for the present work are kindly provided by the Computing Center of National Cheng Kung University.

REFERENCES

1. N. Seki, S.Fukusako and M. Nakoroka, Experimental study on natural convection heat transfer with density inversion of water between two horizontal concentric cylinders, *ASME Trans. J. Heat Transfer* **97,** 556–561 (1975).
2. D. S. Lin and M. W. Nansteel, Natural convection in a vertical annulus containing water near the density maximum, *ASME Trans. J. Heat Transfer* **109,** 899–905 (1987).
3. C. J. Ho and Y. H. Lin, Natural convection of cold water in a vertical annulus with constant heat flux on the inner wall, *ASME Trans. J. Heat Transfer* **112,** 117–123 (1990).
4. C. J. Ho and F. J. Tu, Laminar mixed convection of cold water within a vertical annulus with a heated rotating inner cylinder, *ASME Trans. J. Heat Transfer* **114,** 418–424 (1992).
5. R. C. DiPrima and H. L. Swinney, Instability and transition in flow between concentric rotating cylinders. In *Hydrodynamic Instabilities and the Transition to Turbulence* (Edited by H. L. Swinney and J. P. Gollub), pp. 139–180. Springer, Berlin (1985).
6. D. K. Anson, T. Mullin and K. A. Cliffe, A numerical and experimental investigation of a new solution in the Taylor vortex problem, *J. Fluid Mech.* **207,** 475–487 (1989).
7. G. de Vahl Davis, E. Leonardi and J. A. Reizes, Convection in a rotating annular cavity. In *Heat and Mass Transfer in Rotating Machinery* (Edited by D. E. Metzger and N. H. Afgan), pp. 134–142. Hemisphere, Washington, D.C. (1984).
8. M. A. Hessami, G. de Vahl Davis, E. Leonardi and J. A. Reizes, Mixed convection in vertical annulus, *Int. J. Heat Mass Transfer* **30,** 831–848 (1987).
9. K. S. Ball and B. Farouk, On the development of Taylor vortices in vertical annulus with a heated rotating inner cylinder, *Int. J. Numer. Meth. Fluids* **7,** 857–867 (1987).
10. K. S. Ball and B. Farouk, Bifurcation phenomenon in a Taylor–Couette flow with buoyancy effects, *J. Fluid Mech.* **97,** 479–501 (1988).
11. K. S. Ball and B. Farouk, A flow visualization study of the effects of buoyancy on Taylor vortices, *Phys. Fluids A* **1,** 1502–1507 (1989).
12. K. S. Ball, B. Farouk and V. C. Dixit, An experimental study of heat transfer in a vertical annulus with a rotating inner cylinder, *Int. J. Heat Mass Transfer* **32,** 1517–1527 (1989).
13. B. Gebhart and J. Mollendorf, A new density relation for pure and saline water, *Deep-Sea Res.* **24,** 831–848 (1974).
14. B. P. Leonard, A convectively stable, third-order accurate finite difference method for steady two-dimensional flow and heat transfer. In *Numerical Properties and Methodologies in Heat Transfer* (Edited by T.M. Shih), pp. 211–226. Hemisphere, Washington, D.C. (1983).